Evaluation of a new X-band weather radar for operational use in south Sweden

Seyyed Hasan Hosseini, Hossein Hashemi, Ronny Berndtsson, Nicholas South, Henrik Aspegren, Rolf Larsson, Jonas Olsson, Andreas Persson and Lisa Olsson

ABSTRACT

The performance of a new type of X-band weather radar (WR) for Sweden during a pilot run is studied. Compared to the conventional C-band WRs, the X-band WR covers a smaller area but with a higher spatiotemporal resolution, making it suitable for urban hydrological applications. Rainfall estimations from different elevation angles of the radar (levels) are compared at one-minute and single-event timescales with the observations of several rain gauges at different ranges using hyetographs. In general, the estimations aligned well with observations and the best match appeared for ranges as long as 5–10 km. Seemingly, radar estimations suffered from overshooting of lower lying showers by higher level scans in longer ranges (19–30 km) and from the reflectivity contamination due to moving objects in short ranges (<1 km). Also, the effective range of the radar dropped sharply for the moments when a cloudburst was located over the radar. Although various sources of error could affect the X-band WR rainfall estimates, higher resolution spatiotemporal rainfall monitoring for wider areas will benefit from an integration of data from a network of X-band WRs.

Key words | areal rainfall, attenuation, dual polarization, hyetograph, mass conserving remapping, WR-2100

Seyyed Hasan Hosseini (corresponding author)
Hossein Hashemi
Ronny Berndtsson
Rolf Larsson
Water Resources Engineering, LTH,
Lund University,
P.O. Box 118, SE-221 00 Lund,
Sweden
E-mail: *hasan.hosseini@tvrl.lth.se*

Seyyed Hasan Hosseini
Hossein Hashemi
Ronny Berndtsson
CMES, Lund University,
P.O. Box 201, SE-221 00 Lund,
Sweden

Seyyed Hasan Hosseini
Water Engineering, Faculty of Agriculture,
University of Tabriz,
Postal Code 5166616471, Tabriz,
Iran

Nicholas South
Lisa Olsson
VA SYD,
P.O. Box 191, SE-201 21 Malmö,
Sweden

Henrik Aspegren
Sweden Water Research, The Joint R&D company of NSVA, Sydvatten and VA SYD, Ideon Science Park,
Scheelevägen 15, SE-223 70 Lund,
Sweden
and
Department of Chemical Engineering LTH,
Water and Environmental Engineering,
P.O. Box 124, SE-221 00 Lund,
Sweden

Jonas Olsson
Swedish Meteorological and Hydrological Institute,
SE-601 76 Norrköping,
Sweden

Andreas Persson
Lund University GIS Centre,
P.O. Box 117, SE-221 00 Lund,
Sweden

INTRODUCTION

Accurate rainfall data are undoubtedly a fundamental requirement to evaluate water availability and hazards for the environment and society across an area of interest

doi: 10.2166/wst.2020.066

such as an urban watershed. In addition, the impact of climate change with increased extreme rainfall events in many parts of the world calls for the development of more efficient hydrological modelling. Based on the characteristics of urban hydrology such as quick response time and runoff due to a higher percentage of impervious surfaces, it is evident that higher temporal and spatial resolution rainfall data are essential for input to hydrological models to simulate runoff accurately and eventually, for proper design of the drainage system. From previous studies, it is well known that the uncertainty in urban hydrological models is mainly due to the errors in rainfall data (Willems 2001; Thorndahl *et al.* 2008; Schellart *et al.* 2012).

Rainfall can either be directly measured fairly accurately at a point on the ground using an instrumented site with rain gauge or be indirectly estimated aloft by the recent technological advancements in the field of remote sensing techniques such as weather radar (WR). Rain gauges that traditionally provide required datasets for hydro-meteorological applications may not well reflect the distribution of areal rainfall, depending on the density of the rain gauge network and the complexity of the train (Hiebl & Frei 2018). Remote sensing of hydrometeors, using the WR technique, provides a unique wealth of information on the short-term areal precipitation, of use for various hydro-meteorological applications. There are three frequency bands commonly used for rainfall estimation by WRs. Compared to the conventional C- and S-band WRs, which are widely used for weather surveillance, the X-band WR covers a smaller area but with a higher spatiotemporal resolution. As a result, recent studies suggest the use of observations at X-band frequency as an alternative or an addition to S- and C-band data (Lengfeld *et al.* 2013, 2014; Trabal *et al.* 2013) to fulfil the requirements of urban drainage system modelling, rainfall–runoff models of rural river systems, hydraulic simulations, detailed information on extreme events, etc.

More complex error characteristics and increase of higher intensity rain measurement uncertainty for radar data as compared to rain gauges traditionally limit the operational applications of radar data in urban hydrology (Einfalt *et al.* 2004). Due to the ongoing advancement in radar software, signal, and data processing as well as in data analysis methods and modelling, the number of urban hydrological studies relying on radar has increased immensely during the last decades (Thorndahl *et al.* 2017). Especially, dual-polarization radars are now an important tool for quantitative precipitation estimation (QPE) by providing more accurate physical information of hydrometeors as well as enabled methods for rain attenuation detection and rain drop size distribution (DSD) dynamics as compared to the single-polarization radar QPE (Cifelli & Chandrasekar 2010; Lim *et al.* 2013). Along this line, Kumjian (2013) provides a descriptive review of the polarimetric radar variables, while Simpson & Fox (2018) assess the performance of QPE using single- and dual-polarization radar equations as a function of range for different rainfall regimes (summer and winter). Although dual-polarization techniques and applications have been introduced to S- and C-band WRs for several decades, higher frequency polarimetric X-band WRs are now becoming popular for the sake of higher resolution QPE applications (Wang & Chandrasekar 2010; Lim *et al.* 2013; Li & Willems 2017). Given the existence of various error sources that affect radar estimates (e.g. signal attenuation, beam blockage, etc.), studies have employed different approaches to identify error sources (Van de Beek *et al.* 2016) and improve the QPEs using different combinations of X-band WR data with data from rain gauges (Wang *et al.* 2013) or radars with other frequencies (Lengfeld *et al.* 2018). Combining data from different sources requires remapping using so-called precise, mass-conserving methods as described by Sharif & Ogden (2014). Regardless of the methodological diversities, there is a consensus among the radar community that suitable precipitation data for urban hydrological applications are approximately a spatiotemporal resolution of about 1 km and 1–2 min (Einfalt *et al.* 2004; Ochoa-Rodriguez *et al.* 2015). A volumetric accuracy of less than three percent and 20 years, or more, of recording without missing data are also required (Einfalt *et al.* 2004; Thorndahl *et al.* 2017).

In Sweden, the Swedish Meteorological and Hydrological Institute (SMHI) observes countrywide rainfall using a C-band WR network, with outputs generally at 15 min and 2 km resolution. A product based on these observations (at the same resolution), mainly designed for hydrological applications, is the HIPRAD data set obtained by adjusting QPEs to gridded observations from the national meteorological network (Berg *et al.* 2016). As for a potential augmentation for precipitation monitoring in urban hydrology applications, the southern Swedish water utility company, VA SYD, in collaboration with Lund University, has initiated a test of a new compact type dual polarimetric X-band WR for Sweden (South *et al.* 2019). The purpose of the test was, apart from expanding knowledge about how to measure and project precipitation data, to obtain an in-depth understanding of how an X-band WR can be implemented as part of operation of a water utility. Some

important advantages of such an X-band WR over the traditional C-band WR include smaller cost and size, lower power consumption, and higher spatiotemporal resolution.

Presenting an overall performance of the new WR using a pilot test in summer 2018, the paper aims at introducing the capabilities of the WR in QPE and discussing error sources that could affect it. Further, this study aims to investigate the potentials for improving high-resolution precipitation monitoring taking advantage of the polarimetric X-band WR. The study focuses on case study rainfall events with different intensity, rainfall distribution over time, and event duration to evaluate different potential error sources affecting the QPE as related to the rainfall pattern. In addition, rain gauge observations at several ranges (0–30 km) and radar data from radar scanning in different elevation angles (2–8°) are used to attribute the appeared errors to the range and elevation of the targeted sampling volume while the use of lowest radar level (0.5°) is recommended to mitigate errors due to evaporation and wind drift (Simpson & Fox 2018). Finally, by looking into the short-term variability of local rain and applying a mass-conserving interpolation method, the study provides a ground to analyze the uncertainty of the radar-gauge comparisons.

MATERIALS AND METHODS

Overview of the pilot test and radar characteristics

On 3 July 2018, a new WR device of the Compact Dual Polarimetric X-band Doppler type (FURUNO WR-2100) was installed at the geographic location of 55.67 °N and 13.36 °E in Dalby, southern Sweden. As a pilot survey, it was operated for 72 days (3 July 2018 14:14 to 12 September 2018 12:21 UTC). Accordingly, one binary data file with a fixed predefined format was automatically written for each scan of radar (i.e. 360° rotation round to azimuth) right into a server with scn file extension (hereinafter, scn file). Four of these files were uploaded every minute to the server each equivalent for a radar scan in a given elevation angle (level), which was 2, 4, 8, or 10°. Every scn file was about 15.2 MB, and, in total, the size of stored data was approximately 6.48 TB for the whole operational time period. The temporal resolution for the radar was considered 1 min, equal to the radar revisit time, while the spatial resolution was naturally variable by range. A sampling volume of the radar is specified by azimuthal and range/radial resolution; thus, it expands by range according to the radar beam width. For this pilot case, the radial resolution, which is practically governed by the storage and data transmission limitations, was fixed at 50 meters, and the number of range direction data for every scan-line (azimuth angle) was 1,002, thus the radar collected data in maximum 50.1 km ($50 \times 1{,}002$) of range. As an example, the equivalent rectangle for a radar bin (a radar bin is the projection of a radar sampling volume on the Cartesian plane) in the range of 1 km was 50×47 m^2 (0.24×10^{-2} km^2) while it increased to 50×471 m^2 (2.4×10^{-2} km^2) in the range of 10 km for the beam width of 2.7°. The total number of sweeps (number of scan-lines) was 887 for a complete scan round to azimuth. Therefore, on average, the radar stored data for a scan-line were every 0.406 degree (=360/887) of azimuthal change (sweep). In total, each scn file contained data from 888,774 ($887 \times 1{,}002$) radar bins.

Radar algorithms for precipitation estimation

QPE using WR is usually calculated based on reflectivity data, an important and basic parameter that is measured as an average value of the returned power of particles in a sampling volume by the radar. Reflectivity is an indirect measure of the raindrop size (diameter), number, and concentration, represented by the unit of mm^6 m^{-3} (the sixth power of raindrop diameters per volume of space). Although the actual DSD and rain type (liquid, ice, or mixed) are unknown quantities to the radar, there are standard formula such as $Z = aR^b$ used for determining the relationship between precipitation intensity (R) and the reflectivity factor (Z) where a and b are parameters. The best known, and still one of the most used ones, is the Marshal-Palmer relationship, where $a = 200$ and $b = 8/5 = 1.6$. Since the atmosphere is a dynamic target, the reflectivity measurements are based on some assumptions (e.g. even distribution of many drops throughout the sampling volume), which are seldom met in reality. Therefore, in rainfall intensity measurement based on a fixed radar equation, there is a degree of uncertainty that could be variable by location and time according to the present type/status of rainfall. As a result, the QPE are practically presented by applying a bias correction procedure according to the rainfall observations through the terrestrial rain gauge or disdrometer networks. In this pilot test, however, we compared the QPE based on a fixed relationship (described in the following) assuming that a comparable ground was available for the chosen locations in the radar range during the rainfall events and the comparisons could be attributed to the radar performance.

The simplest precipitation estimation method available by the WR in Dalby is based on Equation (1), which is a rewritten form of the Marshal-Palmer equation where $dBZ_h = 10\ \mathrm{Log}_{10}\ Z_h$ and subscript h for the reflectivity factor (Z) indicates the horizontal polarization of the reflectivity. Accordingly, R_{zh} (in mm h^{-1}) is the rainfall intensity estimation based on the radar reflectivity data from the horizontal polarization.

$$R_{zh}\left[\frac{mm}{hr}\right] = \left(\frac{10^{(dBZ_h/10)}}{200}\right)^{\frac{5}{8}} \quad (1)$$

No loss in signal intensity (attenuation) between the target and the radar is another assumption for applying the radar reflectivity data for QPE as described above. In reality, radar wavelengths, especially in X-band frequency, are subject to significant attenuation in the atmosphere, and this issue needs to be addressed. Attenuation correction methods established based on dual polarization radar variables can be helpful for this purpose. A polarimetric radar is capable of comparing the amplitude and phase of the received signals at both horizontal and vertical polarization, which could be different for oblate, non-spherical drops. For the Dalby WR, the rainfall attenuation was corrected by a general built-in method to the radar (described in the following) using the radar product K_{dp}, the specific differential phase shift. K_{dp} is defined as the range derivative of Φ_{dp}, which is the differential phase (between two polarizations), along the wave propagation path. Φ_{dp} is measured in radian (or degree) while K_{dp} is in $^\circ\ \mathrm{km}^{-1}$. The theory behind this attenuation correction method is that K_{dp} is based on phase measurements, not signal intensity, and it is not affected by attenuation (Kumjian 2013). According to Bringi & Chandrasekar (2001), a linear relationship between the specific attenuation, A (in dB km^{-1}) and K_{dp} (in $^\circ\ \mathrm{km}^{-1}$) can present an excellent approximation at C- and X-band frequencies; in a complete form, A_h (specific attenuation at horizontal) $= \alpha\, K_{dp}^{m}$ and A_{dp} (specific differential attenuation between horizontal and vertical) $= \beta\, K_{dp}^{n}$ where m and n are constants, typically close to one, and α and β are coefficients that generally increase by frequency. Since Dalby WR applies a 9.4 GHz frequency, the radar correction method uses default coefficients of 0.233 and 0.030. Therefore, the specific attenuations and corrected reflectivity values for every sampling volume i are calculated as:

$$A_h(i) = 0.233 \times K_{dp}(i)^{1.020} \quad (2)$$

$$A_{dp}(i) = 0.030 \times K_{dp}(i)^{1.293} \quad (3)$$

$$Z_{h\_cor}(i) = Z_h(i) + 2 \times \sum_{i=0}^{i} A_h(i) \times \frac{\Delta r}{1000} \quad (4)$$

$$Z_{dr\_cor}(i) = Z_{dr}(i) + 2 \times \sum_{i=0}^{i} A_{dp}(i) \times \frac{\Delta r}{1000} \quad (5)$$

where Δr is the range increment (100 m by default), and Z_{h_cor} and Z_{dr_cor} are corrected reflectivity in the horizontal and corrected differential reflectivity (between horizontal and vertical polarizations), respectively, where $dBZ_{dr} = 10\ \mathrm{Log}_{10}\ (Z_h/Z_v)$.

It is noteworthy that the coefficients' values for Equations (2) and (3) are recommended as a result of the temperature-averaged (0–30 °C) fits based on scattering simulations using gamma DSDs over a wide frequency range (2.8–19.35 GHz) as presented by Jameson (1992). Although A can vary by a factor of 1.5–2.0 in the 0–30 °C temperature range, this dependency is weak for higher frequencies (bands $\geq$ 10 GHz) (Bringi & Chandrasekar 2001). However, applying accurate coefficients in Equations (2) and (3) still results in an approximate attenuation correction because K_{dp} itself is noisy and insensitive at very small drops (<0.5 mm), while A is possible in accordance with the total content of water at any size in space (Bringi & Chandrasekar 2001). Non-meteorological echoes are also a cause of noisy K_{dp}. The correlation between the horizontal and vertical polarization signal (ρ_{hv}) for favorable targets (e.g. rain) generally results in a high ρ_{hv} (>0.95). So, for the polarimetric correlation less than a certain limit (i.e. 0.90) K_{dp} is not calculated. ρ_{hv} values for the Dalby WR are corrected using a built-in method for the signal-to-noise ratio as described in Shusse *et al.* (2009).

Upon the calculation of corrected Z values using Equations (4) and (5), Dalby WR calculates precipitation intensity R as a function of both Z_{h_cor} and Z_{dr_cor} (in dB) through Equation (6).

$$R_{cor}\left[\frac{mm}{hr}\right] = 0.013 \times 10^{0.0869 \times Z_{h\_cor} - 0.429 \times Z_{dr\_cor}} \quad (6)$$

Other possible combinations for precipitation estimation by the WR in Dalby are realized by direct use of K_{dp} either with the corrected differential reflectivity as:

$$R_{cor} = 26.0 \times K_{dp}^{0.883} \times 10^{-0.0988 \times Z_{dr\_cor}} \quad (7)$$

or as an individual variable in the form of:

$$R_{cor} = c_1 \times c_2 \times K_{dp}^{c_3} \quad (8)$$

with default values of 19.6, 0.825, and 1.20 for c_1, c_2, and c_3, respectively.

As discussed shortly before, K_{dp} and, to some extent, Z_{dr} are generally noisy for low reflectivity Z_h. Therefore, in application of the above three algorithms, especially for Equation (8) when K_{dp} and Z_h are smaller than a threshold, rainfall is estimated only using the Z_h. The threshold for the WR in Dalby is by default 0.3 ° km^{-1} and 30 dB. For such conditions, the attenuation correction parameter Kr in range r is calculated by the radar built-in process as function of R_{zh}, from Equation (1), in-between the radar and targeted sampling volume as:

$$Kr\,(r) = 0.013 \times \int_0^r R_{zh}^{1.15}\, dr \quad (9)$$

and the corrected rainfall intensity can be presented as:

$$R_{zh\_cor} = \left(\frac{10^{\frac{dBZ_h + Kr}{10}}}{200}\right)^{\frac{5}{8}} \quad (10)$$

Beam blockage (BB) due to ground clutter is another important source of error in QPE. A complete BB (CBB) in some azimuthal angles is sometimes inevitable at special locations such as rugged mountainous regions but it was not the case for the Dalby WR. A more usual form of blockage is partial BB (PBB). False echoes due to PBB can be addressed by applying certain algorithms (e.g. Shakti & Maki 2014). There is not any procedure for clutter compensation built-in to the WR in Dalby. Therefore, no correction for the WR data was employed in this study. However, the radar data were investigated for the existence of BB during the pilot run.

Evaluation of QPE vs. rain gauge measurements

For a quantitative evaluation, the radar rainfall estimations at different levels were compared with the observations of rain gauges at different ranges at one-minute and single-event time scale. Data from rain gauges, mostly located in the municipalities of Malmö and Lund, were collected from the regional water utility company, VA SYD. Figure 1 shows a map of the spatial distribution of the rain gauges studied in this paper in the 50 km radius coverage of the radar. While the radar estimates instantaneous rainfall intensity (an intensity sample for a minute), the rain gauges accumulate and measure rainfall until the minimum amount of 0.2 mm is reached. Because of this intrinsic difference between the two data sets (gauge and radar), their hyetographs (i.e. graphs of rainfall intensity distribution over time) may not match each other even for an ideal estimation by the radar. Therefore, for visualizing the comparison between radar estimation and gauge observation, cumulative hyetographs are additionally presented. As the first 0.2 mm record of an event for the rain gauge could actually be accumulated from a few minutes before the time of record by the rain gauge, the equivalent radar data for a given event were selected from a few minutes before the first record of the event by the rain gauge. Thus, the beginning of the equivalent radar period was one minute after the first zero value in the time series of radar data in the period before the first 0.2 mm record of the event.

Evaluation of instantaneous complexity of local rain

In addition to the temporal issue discussed earlier, the idea behind the evaluation of the radar QPE based on the radar-gauge data comparison is that the rainfall at a point (i.e. rain gauge) is an ideal representation of the radar bin that contains it. This is true if the variability of the rainfall intensity within the radar bin is low, which is seldom possible especially for radar bins associated with large ranges. In order to evaluate this uncertainty, we compared the spatial variation of radar estimations from radar bins close to each other. Basically, since the azimuthal change for every sweep of the radar is a few times smaller than the radar beam width, there are obviously overlaps between the radar bins from consecutive scan-lines. Inspired by Sharif & Ogden (2014), we applied a geometrically precise interpolation method considering data from all radar sampling volumes (alternative bins) that contribute partially or totally within a given bin, by giving each a weight proportion to their spatial (areal, on the plane) contribution. Comparison of the interpolated values with the raw, single-bin data provided a basis to indicate instantaneous complexity of local rainfall.

RESULTS AND DISCUSSION

Evaluation of high intensity rainfall event

Table 1 presents characteristics of a case study intense rainfall event observed by six rain gauges at different ranges of the radar (~1–30 km) during the study period. For instance, the rain gauge at Södra Sandby, at a range of 5.6 km, recorded 24.6 mm rainfall during the 68-min event (from

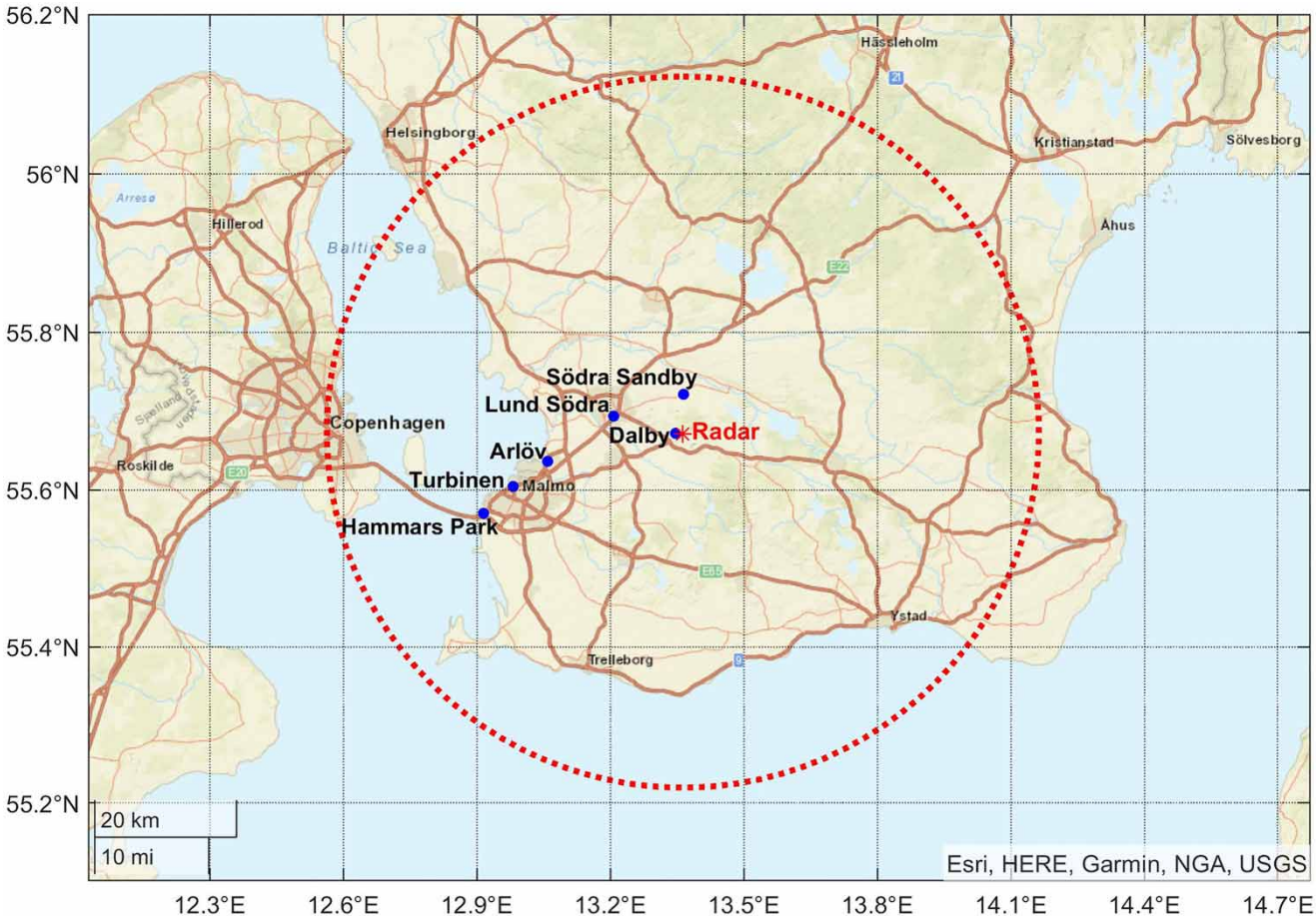

Figure 1 | Location of the X-band WR at Dalby (red star) and the selected VA SYD's rain gauges (blue points) within the 50 km range radius (large dashed ring). Please refer to the online version of this paper to see this figure in colour: http://dx.doi.org/10.2166/wst.2020.066.

00:47 to 01:54 UTC + 2 on 10 August 2018), which is equivalent to a 0.36 mm min^{-1} average rainfall intensity. It is noted that the period of this event for each rain gauge (start and end time) was selected so that the time interval between two consecutive 0.2 mm recordings for a given rain gauge was not more than 10 min.

Figure 2 illustrates the rainfall intensity variations (Figure 2(a)) as well as the cumulative hyetographs (Figure 2(b)) based on the rain gauge observations and the radar estimations for the event on 10 August 2018, described earlier in Table 1. According to both Figure 2(a) and 2(b), the radar estimations aligned generally well with the gauge

Table 1 | Rainfall event characteristics observed by six rain gauges on 10 August 2018

Location				Rainfall event				
Station name	Lat. (°N)	Long. (°E)	Range (km)	Start time (UTC + 2)	End time (UTC + 2)	Total amount (mm)	Mean intensity (mm/min)	Max intensity (mm/min)
Dalby	55.67	13.35	0.8	00:40	01:50	19.4	0.27	1.6
Södra Sandby	55.72	13.36	5.6	00:47	01:54	24.6	0.36	2.2
Lund Södra	55.67	13.21	9.9	00:27	01:59	25.8	0.27	1.4
Arlöv	55.64	13.06	19.3	00:18	01:53	19.8	0.21	1.4
Turbinen	55.60	12.98	24.9	00:11	01:51	21.4	0.21	1.2
Hammars Park	55.57	12.91	30.1	00:04	01:53	21.8	0.20	1.6

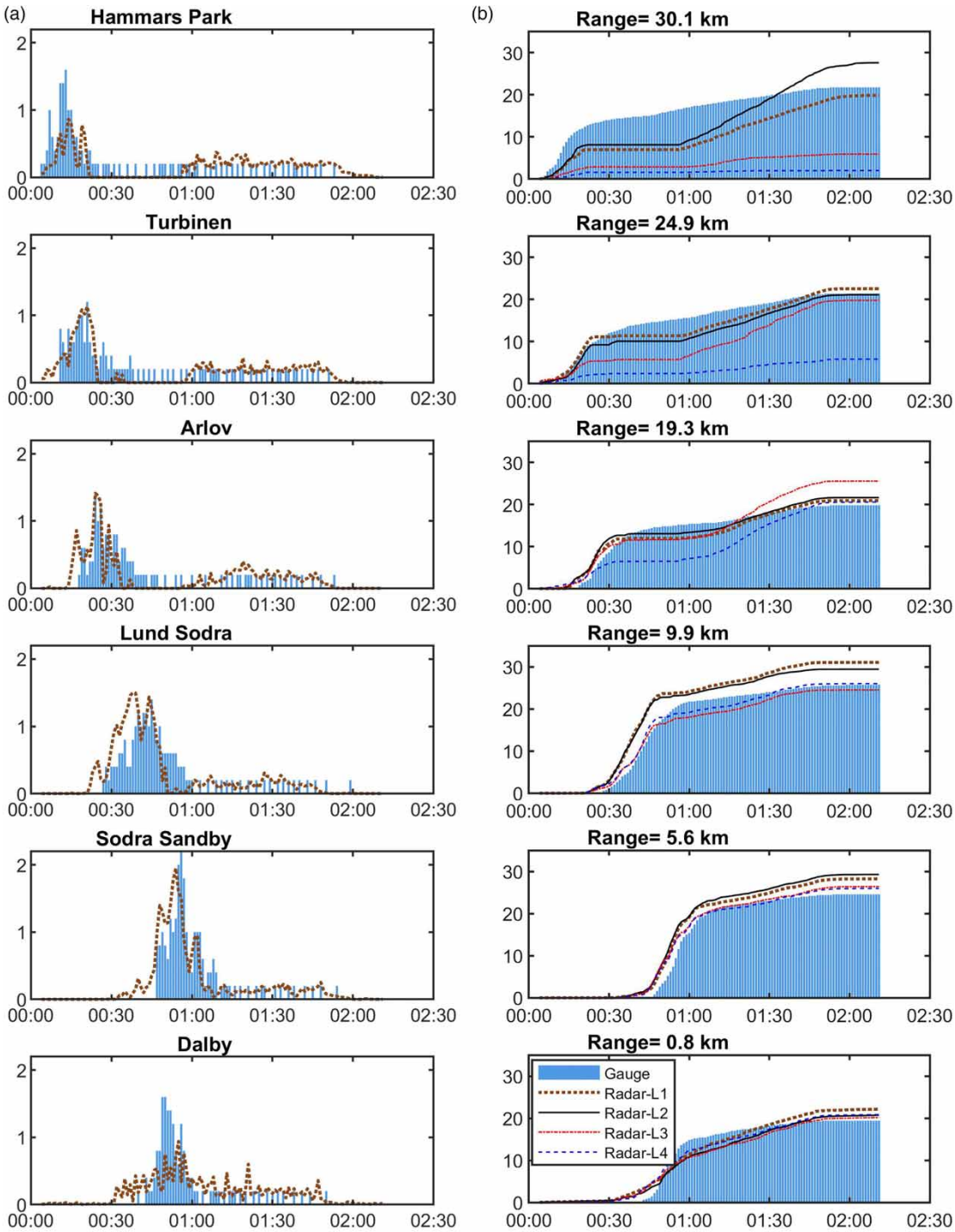

Figure 2 | Comparison of rain gauge observations and radar estimations at different levels (L1 to L4) for six different locations during 00:00 and 02:10 UTC + 2 on 10 August 2018 for rainfall intensity (a) and cumulative hyetographs (b).

observations, suggesting a potential for the radar bias correction against the observations. However, these figures also reveal an interruption of radar data collection, more obvious for the locations of the Arlöv, Turbinen, and Hammars Park rain gauges, from all radar levels between 00:20–01:00, although the rain gauges continued to record rainfall. As can be followed from the graphs in Figure 2(a), this interruption for each station started a few minutes after the high

intensity rainfall passed the rain gauge toward the location of the radar. As a result, the front of the rain (with a high intensity) positioned between the radar and the rain gauge. Thus, the radar signals were attenuated and caused an error in the rainfall estimation for this period.

By investigating the areal rainfall maps from the radar, it was evident that the effective range of the radar dropped sharply when a cloudburst was located over the radar. This is a general flaw of the X-band WRs that is suggested to be resolved by a network of X-band radars, assuming that while one radar suffers an interruption, other ones may gather information at different angles. As discussed by South *et al.* (2019), the data from the C-band WR network of the SMHI showed to be less affected by the attenuation due to heavy rain, and as a result could also provide information for the X-band WR monitoring.

Figure 2(b) shows that the difference between the estimated rainfall at different levels increased by range. In addition, radar scans at higher levels (level 3 and, especially, level 4) could not properly detect the actual rainfall for ranges of 25 to 30 km, where Turbinen and Hammars Park stations are located, respectively. This can be related to the overshooting of lower-lying showers relative to the position of the radar sampling volume, as it obviously rises by range in proportion to the radar elevation angle. However, it seems that the radar scans at Level 3 and Level 4 resulted in a better estimation of the rainfall as compared to observations at mid-ranges (~5–10 km) where Södra Sandby and Lund Södra stations are located (Figure 2(b)).

Evaluation of lower intensity rainfall event

To further evaluate rainfall estimation obtained by the X-band WR, another rainfall event observed on 13 August 2018 was studied (Table 2). Compared to the event on the 10th of August (Table 1), the event on the 13th was associated with a smaller amount of rainfall distributed over a longer period. Therefore, it is expected that the error caused by the signal attenuation due to the heavy rain was limited and radar estimations could be examined for other error sources. This low-intensity rainfall event contained dry periods of about 30 min for all stations (Figure 3; between 00:50 and 08:00 UTC + 2 on 13 August 2018).

Figure 3 illustrates rainfall intensity variation (Figure 3(a)) and cumulative hyetographs (Figure 3(b)) for the six different locations presented in Table 2. According to Figure 3(b), at the farthest location to the radar (Hammars Park at range 30.1 km), the cumulative hyetographs of the estimated rainfall at level 1 and 2 displayed more or less the same variation over the entire event, except for the appearance of a relatively high intensive period at about 04:00. The discrepancy for this period is even more obvious at the Turbinen location (Figure 3(b)), where radar estimation was not successful at any of the levels. The inability of the radar during this abrupt change of rainfall intensity could be related to the discrete sampling feature associated to the time it takes for the radar beam to revisit a given point in space. According to the cumulative hyetographs for the two rain gauges located at Turbinen and Hammars Park (Figure 3(b)), the radar scanning at level 3 and 4 detected almost no rainfall. Therefore, it is expected that the overshooting of the lower lying showers by the higher level scans of the radar at long ranges, which was previously discussed for the event on the 10th of August, was also the case for the event on the 13th. Overshooting might also be partially responsible for the underestimation that appeared at the lower levels of the radar (Figure 3(b)). By this assumption, the lower underestimation of rainfall for Hammars Park station compared to the Turbinen station, while it is at a longer range, could be explained by

Table 2 | Rainfall event characteristics observed by six rain gauges on 13 August 2018

Location				Rainfall event				
Station name	Lat. (°N)	Long. (°E)	Range (km)	Start time (UTC + 2)	End time (UTC + 2)	Total amount (mm)	Mean intensity (mm/min)	Max intensity (mm/min)
Dalby	55.67	13.35	0.8	00:56	07:51	14.6	0.035	0.4
Södra Sandby	55.72	13.36	5.6	01:11	07:51	12.6	0.031	0.4
Lund Södra	55.67	13.21	9.9	01:04	07:59	13.8	0.033	0.4
Arlöv	55.64	13.06	19.3	00:53	06:56	20.8	0.057	0.8
Turbinen	55.60	12.98	24.9	01:00	07:25	18.8	0.049	1
Hammars Park	55.57	12.91	30.1	01:04	07:05	10.6	0.029	0.2

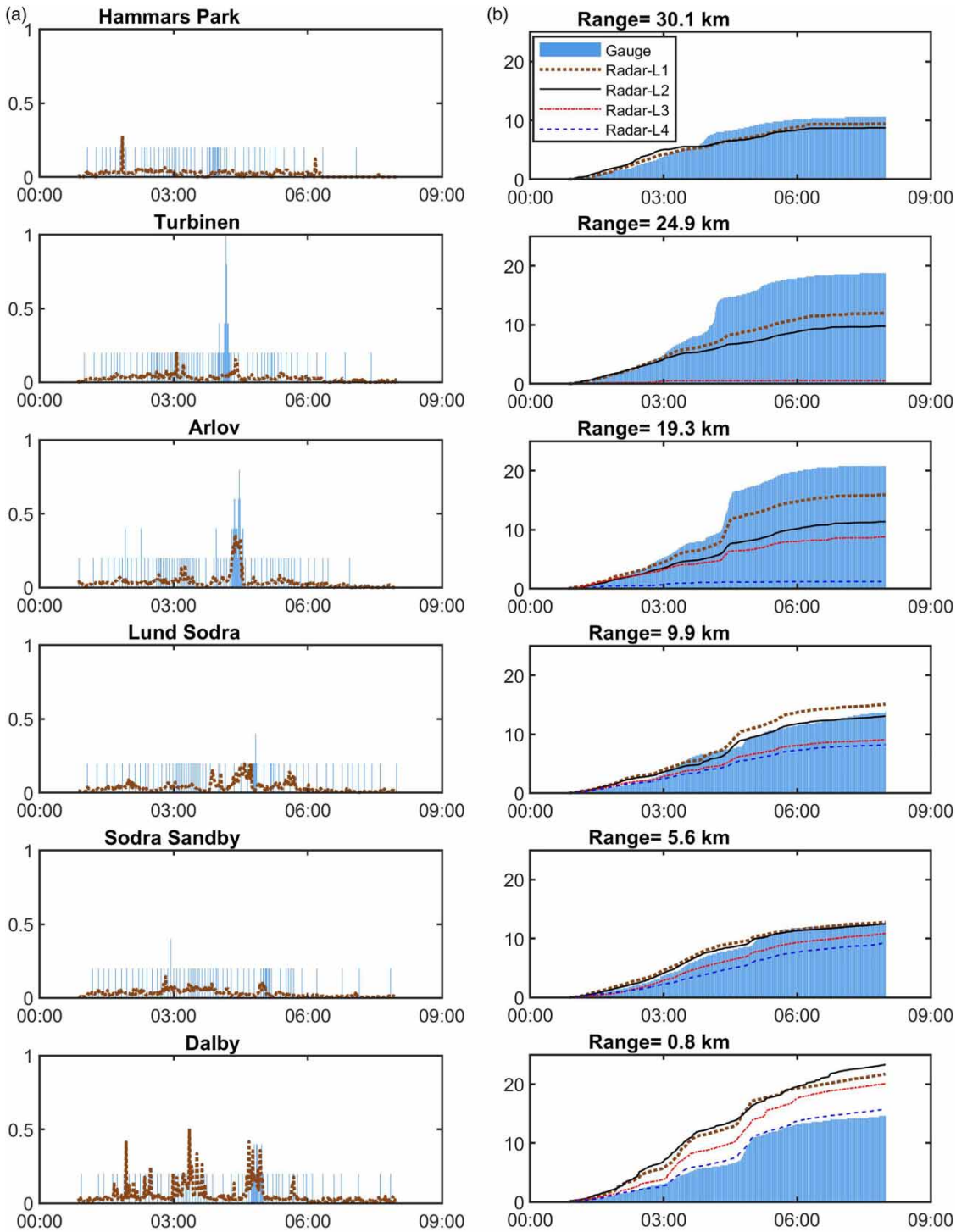

Figure 3 | Comparison between rain gauge observations and radar estimations at different levels (L1 to L4) for six different locations during 00:50 and 08:00 UTC + 2 on 13 August 2018 for rainfall intensity and (a) and cumulative hyetographs (b).

the fact that the observed rainfall at Hammars Park was lower than at Turbinen. If the event for Hammars Park had continued with the same intensity as for Turbinen, larger underestimation could have been present.

On the other hand, neither the overshooting nor the attenuation due to heavy rain could explain the difference between rainfall estimation at different radar levels for the shortest range (0.8 km), where Dalby station is located (Figure 3(b)). Actually, it is difficult to accept that the estimation at the different levels for the Dalby station in Figure 3(b) reflects actual vertical profiles of rainfall due to the fact that the vertical distance between the levels at such a short range (<1 km) is quite small. Instead, this could be related to the reflectivity contamination caused by a moving object such as the rotating blades of wind turbines (Mishra & Chandrasekar 2010), leaves of trees moved by the wind, etc. Such an object may also cause a multi-path scattering of the signals before returning to the radar, which cannot be easily filtered out by the usual clutter removing for most applications. As a result, more rainfall than is actually present is detected by the radar, especially at lower levels where the chance for visiting an object close to the ground is higher.

The rainfall intensities at the lowest level for the closest station to the radar; that is, Dalby, are more jagged compared to the same event for the stations located at longer range (Figures 2(a) and 3(a)). This might be due to the existence of moving objects. A more pronounced effect of this at the Dalby station is supported by the fact that the radar sampling volume is quite small at very short ranges and any misleading reflectivity from a moving object (e.g. a bird) of a certain size could contribute with higher weight to the rainfall estimation of that sampling volume. Anyway, the highest-level scan of the radar (level 4) provided an accurate estimation of rainfall for this location.

As shown by the cumulative hyetographs in Figure 3(b), the radar estimation at level 1 and 2 for a range of 5 and 10 km, where Södra Sandby and Lund Södra stations are located, adequately matched rain gauge observations. Good performance of the radar could also be observed for the rainfall event on the 10th of August (Figure 2(b)). Thus, quantitative rainfall estimation at mid-range (5–10 km) seems to be less affected by both signal attenuation due to heavy rain and by the false detection related to moving objects. However, the best estimation for the mid-range event on the 13th of August was presented by level 2 of the radar (Figure 3(b)), while the scan at higher level (3 and 4) presented the best estimation for the event on the 10th. This fact may suggest that the showers related to the event on the 13th were formed at lower elevations. This supports the assumption that the overshooting by even the lower level scan of the radar was responsible for the considerably high underestimation appearing at the range 19–30 km during this event (Figure 3(b)).

Integration of QPE results

As discussed above, there are several sources of errors influencing the rainfall estimations by the X-band WR. These errors can depend on time and location as well as the characteristics of the areal rainfall present in both time and space. Other important sources of error are related to the raindrop size distribution, ground clutter, false clutter filtering related to the near-zero Doppler velocities, and wet-radome attenuation (Van de Beek *et al.* 2016). More reliable rainfall estimation can be provided by removing effects of as many of these errors as possible by incorporating a wider range of information from the Doppler data and the dual polarimetric variables in the combination of C-band and X-band weather radar data (Lengfeld *et al.* 2016). Moreover, the results show the importance of using an established combination of radar levels for any data adjustment procedure based on different range, intensity, etc. Such a procedure should be capable of a regular update after acquiring new records representing new facets of the variability in the involved processes, which obviously is not a straightforward task.

Uncertainty of estimations

It should be noted that the generally lower accuracy of the radar estimation for larger ranges could be related to the fact that the radar sampling volume expands as the range increases and the assumption of a uniform rainfall for a certain radar bin is less valid. As a result, radar calibration based on rain gauge observations can be biased if the spatial variability of rainfall is so high that a point measurement obtained from a rain gauge is not a good representative of a radar bin containing it.

Comparison of the interpolated values with the raw, single-bin radar data was used to indicate the instantaneous complexity of local rainfall. Since the average sweep change for the radar was almost 0.4°, while the beam width is 2.7°, six pre and six post scan-lines can contribute to a given bin. Figures 4 and 5 show differences between the interpolated and raw radar data for radar bins positioned at 19 and 30 km ranges. As a result, a difference is present for both ranges, but more significant deviation can be observed in Figure 5, which is related to the longer range as compared to Figure 4. This may be due to the fact that a 0.4° sweep is equivalent to 147 m displacement in the 19 km range while it is 209 m in the 30 km range.

The WR in Dalby several times displayed sporadic low-intensity echoes in some specific bins close to the radar

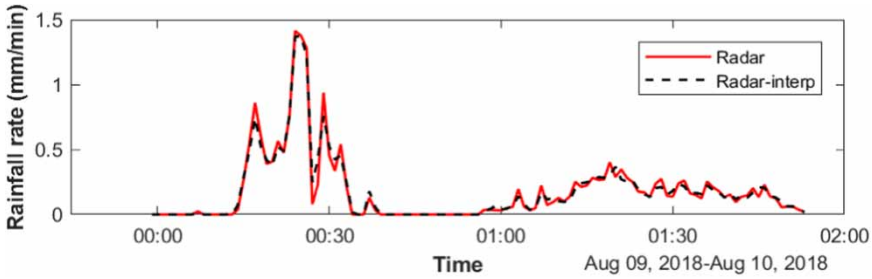

Figure 4 | Difference between raw and interpolated rainfall intensities for the rainfall event on 10 August 2018, in the radar bin containing the Arlöv station at the range of 19 km.

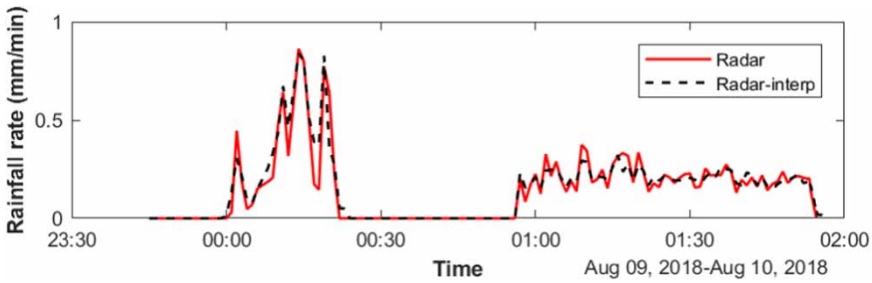

Figure 5 | Difference between raw and interpolated rainfall intensities for the rainfall event on 10 August 2018, in the radar bin containing the Hammars Park station at the range of 30 km.

location and within a 10 km range during clear sky, without any rain or cloud. These echoes are most likely produced by PBB from tall buildings close to the radar or signal contamination due to moving objects; for example, moving wind turbine blades or flying birds. However, these error sources seem to be less important in distorting QPEs as compared to other error sources, such as attenuation during heavy rain and overshooting. Figures 2(b) and 3(b) show the best match between the radar and rain gauge data for the 5–10 km range, while radar bins in this range interval included the highest false, non-rainfall echoes. This may be related to the fact that the radar is sensitive to clear-sky conditions. Another reason can be that the intensity of false echoes is generally lower than echoes from areal rainfall filling. Even if the effect of these errors is negligible for individual rainfall events, failure to remove them may result in uncertainty when using correction methods such as mean field bias. As a result, the clutter removing should be applied to the radar QPEs (Shakti & Maki 2014).

CONCLUSIONS

Various hydro-meteorological applications including rural and urban flood management require accurate short-term areal precipitation data. As a pilot test, a compact new type of ground-based X-band WR was installed for the first time in Sweden and was operated for 72 days. The X-band WR is suitable for urban hydrology applications by providing higher spatiotemporal resolution estimations of rainfall, but for smaller areal coverage, compared to the conventional S-band and C-band WRs.

To evaluate rainfall estimation from the X-band WR, two case study rainfall events (a high-intensive and a low-intensive summer rainfall event) for six rain gauge stations located at different ranges from the radar were studied. It was shown that the estimation of high-intensity rainfall was subject to attenuation due to heavy rain so that gathering of data was practically interrupted, especially at ranges longer than 20 km. For the two investigated rainfall events, overshooting of the lower-lying showers by the higher-level scans of radar (i.e. elevation angles 8 and 10°) caused huge underestimation at ranges as long as 19–30 km. On the other hand, rainfall estimation at short ranges (<1 km), especially by lower-level scans (i.e. elevation angles 2 and 4°), was found to suffer from reflectivity contamination due to moving objects in the radar vicinity, resulting in overestimation. The results of this study showed that the rainfall estimation by the X-band radar in mid-range (~5–10 km) was the most accurate as it was less affected by reflectivity contamination, overshooting, and attenuation due to heavy rain.

In conclusion, higher resolution spatiotemporal rainfall monitoring for wider applications will benefit from the integration of data by a network of X-band WRs, assuming that deficiencies of individual radars can be overcome by a

system of radars. Due to the various sources of error affecting rainfall estimation, however, radar data cleaning is not a straightforward process. It will require detailed studies discriminating between the affecting sources, according to the characteristics of the areal rainfall in time and space. Therefore, more investigations are needed that can combine data of different sources to improve estimation methods. An interesting prospect mentioned above (section Integration of QPE results) is to use local X-band data to improve the quality of the national WR-based products, that way producing an added value also outside the X-band domain.

ACKNOWLEDGEMENTS

The authors appreciate financial support from the Swedish Water & Wastewater Association, SVU (Svenskt Vatten Utveckling). The constructive comments by three anonymous reviewers on the original manuscript is also appreciated. J. Olsson acknowledges additional support from the Swedish Research Council Formas.

REFERENCES

Berg, P., Norin, L. & Olsson, J. 2016 Creation of a high resolution precipitation data set by merging gridded gauge data and radar observations for Sweden. *Journal of Hydrology* **541**, 6–13.

Bringi, V. N. & Chandrasekar, V. 2001 *Polarimetric Doppler Weather Radar: Principles and Applications*. Cambridge University Press, Cambridge, UK, p. 636.

Cifelli, R. & Chandrasekar, V. 2010 Dual-polarization radar rainfall estimation. In: *Rainfall: State of the Science*, Vol. 191 (F. Testik & M. Gebremichael, eds). Geophysical Monograph Series, Washington, DC, pp. 105–126.

Einfalt, T., Arnbjerg-Nielsen, K., Golz, C., Jensen, N.-E., Quirmbach, M., Vaes, G. & Vieux, B. 2004 Towards a roadmap for use of radar rainfall data in urban drainage. *Journal of Hydrology* **299** (3–4), 186–202.

Hiebl, J. & Frei, C. 2018 Daily precipitation grids for Austria since 1961 – development and evaluation of a spatial dataset for hydroclimatic monitoring and modelling. *Theoretical and Applied Climatology* **132** (1–2), 327–345.

Jameson, A. R. 1992 The effect of temperature on attenuation correction schemes in rain using polarization propagation differential phase shift. *Journal of Applied Meteorology* **31**, 1106–1118.

Kumjian, M. R. 2013 Principles and applications of dual-polarization weather radar. Part I: description of the polarimetric radar variables. *Journal of Operational Meteorology* **1** (19), 226–242.

Lengfeld, K., Clemens, M., Münster, H. & Ament, F. 2013 PATTERN: Advantages of high-resolution weather radar networks. In: *Proceedings of the 36th Conference on Radar Meteorology*, Breckenridge, CO, USA.

Lengfeld, K., Clemens, M., Muenster, H. & Ament, F. 2014 Performance of high-resolution X-band weather radar networks – the PATTERN example. *Atmospheric Measurement Techniques* **7** (12), 4151–4166.

Lengfeld, K., Clemens, M., Merker, C., Münster, H. & Ament, F. 2016 A simple method for attenuation correction in local X-band radar measurements using C-band radar data. *Journal of Atmospheric and Oceanic Technology* **33** (11), 2315–2329.

Lengfeld, K., Berenguer, M. & Torres, D. S. 2018 Intercomparison of attenuation correction algorithms for single-polarized X-band radars. *Atmospheric Research* **201**, 116–132.

Li, X. & Willems, P. 2017 Performance of high-resolution quantitative precipitation estimation from a compact dual-pol x-band radar in Belgium with evaluation of different gauge-adjustment techniques. In: *Proceedings of EMS2017 Annual Meeting, Dublin, Ireland*.

Lim, S., Cifelli, R., Chandrasekar, V. & Matrosov, S. Y. 2013 Precipitation classification and quantification using X-band dual-polarization weather radar: application in the hydrometeorology testbed. *Journal of Atmospheric and Oceanic Technology* **30** (9), 2108–2120.

Mishra, K. V. & Chandrasekar, V. 2010 Signal analysis and modeling of wind turbine clutter in weather radars. In: *Proceedings of the 30th IEEE International Geoscience and Remote Sensing Symposium*, pp. 3561–3564.

Ochoa-Rodriguez, S., Wang, L.-P., Gires, A., Pina, R. D., Reinoso-Rondinel, R., Bruni, G., Ichiba, A., Gaitan, S., Cristiano, E. & van Assel, J. 2015 Impact of spatial and temporal resolution of rainfall inputs on urban hydrodynamic modelling outputs: a multi-catchment investigation. *Journal of Hydrology* **531**, 389–407.

Schellart, A., Shepherd, W. & Saul, A. 2012 Influence of rainfall estimation error and spatial variability on sewer flow prediction at a small urban scale. *Advances in Water Resources* **45**, 65–75.

Shakti, P. C. & Maki, M. 2014 Application of a modified digital elevation model method to correct radar reflectivity of X-band dual-polarization radars in mountainous regions. *Hydrological Research Letters* **8** (2), 77–83.

Sharif, H. O. & Ogden, F. L. 2014 Mass-conserving remapping of radar data onto two-dimensional Cartesian coordinates for hydrologic applications. *Journal of Hydrometeorology* **15** (6), 2190–2202.

Shusse, Y., Nakagawa, K., Takahashi, N., Satoh, S. & Iguchi, T. 2009 Characteristics of polarimetric radar variables in three types of rainfalls in a Baiu front event over the East China Sea. *Journal of the Meteorological Society of Japan* **87** (5), 865–875.

Simpson, M. J. & Fox, N. I. 2018 Dual-polarized quantitative precipitation estimation as a function of range. *Hydrology and Earth System Sciences* **22** (6), 3375–3389.

South, N., Hashemi, H., Olsson, L., Hosseini, S. H., Aspegren, H., Larsson, R., Berndtsson, R., Das, R., Marmbrandt, A., Olsson, J. & Persson, A. 2019 *Väderradarteknik Inom VA-Området: Test av Metodik (Weather radar technology within water- and*

wastewater treatment – test of methodology). Report 2019-3, Svenskt Vatten Utveckling, Sweden.

Thorndahl, S., Beven, K. J., Jensen, J. B. & Schaarup-Jensen, K. 2008 Event based uncertainty assessment in urban drainage modelling, applying the GLUE methodology. *Journal of Hydrology* **357** (3–4), 421–437.

Thorndahl, S., Einfalt, T., Willems, P., Ellerbæk Nielsen, J., Ten Veldhuis, M.-C., Arnbjerg-Nielsen, K., Rasmussen, M. R. & Molnar, P. 2017 Weather radar rainfall data in urban hydrology. *Hydrology and Earth System Sciences* **21** (3), 1359–1380.

Trabal, J. M., Colom-Ustariz, J. G., Cruz-Pol, S. L., Pablos-Vega, G. A. & McLaughlin, D. J. 2013 Remote sensing of weather hazards using a low-cost and minimal infrastructure off-the-grid weather radar network. *IEEE Transactions on Geoscience and Remote Sensing* **51** (5), 2541–2555.

Van de Beek, C. Z., Leijnse, H., Hazenberg, P. & Uijlenhoet, R. 2016 Close-range radar rainfall estimation and error analysis. *Atmospheric Measurement Techniques* **9** (8), 3837–3850.

Wang, Y. & Chandrasekar, V. 2010 Quantitative precipitation estimation in the CASA X-band dual-polarization radar network. *Journal of Atmospheric and Oceanic Technology* **27** (10), 1665–1676.

Wang, L.-P., Ochoa-Rodríguez, S., Simões, N. E., Onof, C. & Maksimović, C. 2013 Radar–raingauge data combination techniques: a revision and analysis of their suitability for urban hydrology. *Water Sciences & Technology* **68** (4), 737–747.

Willems, P. 2001 Stochastic description of the rainfall input errors in lumped hydrological models. *Stochastic Environmental Research and Risk Assessment* **15** (2), 132–152.

First received 12 October 2019; accepted in revised form 3 February 2020. Available online 18 February 2020